

Exact static solutions for discrete ϕ^4 models free of the Peierls-Nabarro potential

S. V. Dmitriev,¹ P. G. Kevrekidis,² N. Yoshikawa,¹ and D. J. Frantzeskakis³

¹ Institute of Industrial Science, the University of Tokyo, Komaba, Meguro-ku, Tokyo 153-8505, Japan

² Department of Mathematics and Statistics, University of Massachusetts, Amherst, MA 01003-4515, USA

³ Department of Physics, University of Athens, Panepistimiopolis, Zografos, Athens 15784, Greece

(Dated: December 2, 2024)

We discuss some discrete ϕ^4 models free of the Peierls-Nabarro potential. One of them conserves classical momentum while another conserves energy. We propose a generalization of the method suggested recently in J. Phys. A **38**, 7617 (2005) and Phys. Rev. E **72**, 035602(R) (2005). This way, we identify the full space of available static solutions in such models including those derived recently in Phys. Rev. E **72** 036605 (2005) but not limited to them. These findings are also applicable to standing wave solutions of corresponding discrete nonlinear Schrödinger models. We also study stability of the obtained solutions. As an interesting aside, we derive the list of solutions to the continuum ϕ^4 equation that fill the entire two-dimensional space of parameters obtained as the continuum limit of corresponding space of the discrete models.

PACS numbers: 05.45.-a, 05.45.Yv, 63.20.-e

I. INTRODUCTION AND SETUP

Discrete nonlinear models play a very important role in many physical applications [1, 2]. An important class of these models consists of a few completely integrable lattice equations, such as the Toda lattice [3], the Ablowitz-Ladik lattice [4], and the integrable discrete sine-Gordon lattice [5]. The fact that these lattices possess exact soliton solutions demonstrates that, in principle, discreteness of the host media does not preclude the propagation of localized coherent structures. Moreover, the mobility of soliton-like excitations in discrete media is a key issue in many physical contexts; for instance, the mobility of dislocations, a kind of topological solitons, is of paramount importance in the physics of plastic deformation of metals and other crystalline bodies [6].

A prototypical class of discrete models, relevant to a variety of applications, consists of the Klein-Gordon dynamical lattices [1]. One of the main representatives of this family of models is the so-called ϕ^4 model [7], which features a cubic nonlinearity. This simple power law nonlinearity renders this model a ripe testbed for studying the existence and stability of nonlinear solutions, and comparing their properties in continua and lattices.

In the $(1+1)$ -dimensional continuum framework (and in the absence of spatially dependent external potentials), a solution can be shifted arbitrarily along x by any x_0 (x is the spatial coordinate and $x_0 = \text{const.}$), due to the existing translational invariance. On the other hand, in the discrete system, translational invariance is generically lost and equilibrium static solutions exist for a discrete rather than a continuum set of x_0 [1]. Some of these equilibrium solutions correspond to the energy maxima and are unstable, while others, corresponding to the energy minima, are stable. The difference between such maxima and minima of the energy is typically referred to as the Peierls-Nabarro potential (PNp). It is then of particular interest to develop discretizations that do not feature such energetic barriers. In such cases, one

might expect that the ensuing models would be more faithful representations of their continuum counterparts, regarding both symmetry properties and travelling solution features (even though there are some notes of caution that should be made; see e.g. the discussion of [8]).

In that vein, recently, a number of non-integrable discrete Klein-Gordon equations free of the Peierls-Nabarro potential (PNp-free) has been systematically constructed. The first set of such models which were, by construction, Hamiltonian ones, was obtained by Speight and co-workers [9] using the Bogomol'nyi argument [10]. A second successful attempt led to the construction of momentum-conserving discretizations [11]. It was then demonstrated, surprisingly, that the PNp-free models of that kind conserving both energy and classical momentum do not exist [12]. In the recent work of [13] it was shown that, in all cases, PNp-free discrete Klein-Gordon models can be formulated by using a two-point discrete version of the first integral of a static continuum Klein-Gordon equation. The latter equation is a two-point nonlinear algebraic equation from which the exact static solutions of the three-point discretizations resulting into PNp-free models can be found. This idea was reported independently and almost concurrently in [14] for the particular case of the ϕ^4 field. Another PNp-free model has been very recently proposed in [15]. In the static case, their energy-conserving model is equivalent to the static version of the momentum-conserving model of [13]. The scope of the present work is to extend this methodology in a way that provides the full solution space of the underlying static problem.

Our setting is the following: we consider the Hamiltonian of the ϕ^4 model,

$$H = \int \left[\frac{1}{2} \phi_t^2 + \frac{1}{2} \phi_x^2 + V(\phi) \right] dx, \quad (1)$$

where the field $\phi(x, t)$ depends on the coordinate x and

time t , and the (on-site) potential $V(\phi)$ is of the form

$$V(\phi) = \frac{\lambda}{4}(1 - \phi^2)^2, \quad (2)$$

where the parameter $\lambda = \pm 1$. The corresponding equation of motion is

$$\phi_{tt} = \phi_{xx} + \lambda(\phi - \phi^3) \equiv D(x; t). \quad (3)$$

The above, so-called, ϕ^4 equation supports moving periodic solutions that can be expressed in terms of the Jacobi elliptic functions. The latter can be reduced to localized hyperbolic function solutions (when the elliptic modulus $m = 1$). Bounded solutions of this sort were discussed in the context of structural phase transitions [16] and were used as the starting point for derivation of exact solutions to a discrete ϕ^4 model [15]. In section VII we complete the list of the solutions presented in [15, 16] by providing also the set of unbounded solutions of the present model.

The simplest discretization of Eq. (3) is of the form

$$\ddot{\phi}_n = \frac{1}{h^2}(\phi_{n-1} - 2\phi_n + \phi_{n+1}) + \lambda(\phi_n - \phi_n^3), \quad (4)$$

and it possesses a PNp barrier. However, as mentioned above, one can construct PNp-free discrete Klein-Gordon models by discretizing the nonlinear term $V'(\phi)$ typically over three neighboring points, $V'(\phi) \rightarrow V'(\phi_{n-1}, \phi_n, \phi_{n+1})$, in contrast to the classical discretization $V'(\phi) \rightarrow V'(\phi_n)$. The three-point discretization may be physically meaningful in some settings [17], but is also interesting from the more fundamental point of view of developing PNp-free discretizations and obtaining analytically (or semi-analytically) explicit waveforms of their solutions.

In the following, generalizing the approach developed in [13], we will show how to construct *all possible* exact static solutions to the models of [13] and [15] (see also [11, 14]), including those derived in [15]. This will also lead us to introduce a number of solutions (both localized and extended ones) that, to the best of our knowledge, have not been discussed/analyzed previously, such as the ones that will be termed “inverted” (see below). We will also discuss the stability of the main ones among the obtained solutions for each one of the models of interest (since their stability properties are different).

We also note in passing that while our presentation will be geared towards the ϕ^4 models, the results can equally well be applied to discrete equations of the nonlinear Schrödinger (NLS) type [18], such as e.g. the Ablowitz-Ladik model. In particular, let us consider equations of the form:

$$i\dot{\psi}_n = \frac{1}{h^2}(\psi_{n-1} - 2\psi_n + \psi_{n+1}) + f(\psi_n, \bar{\psi}_n), \quad (5)$$

(where the overbar denotes complex conjugate) with $f(\psi_n \exp(i\theta), \bar{\psi}_n \exp(-i\theta)) = f(\psi_n, \bar{\psi}_n) \exp(i\theta)$ and

$\lim_{h \rightarrow 0} f(\psi_n, \bar{\psi}_n) = -\lambda|\psi|^2\psi$. Then, looking for standing wave solutions of the form $\psi_n = \exp(i\lambda t)\phi_n$, with ϕ_n real, one would obtain the same static problem as above for the standing wave spatial profile ϕ_n . Hence all the discussion given below for the existence of such solutions can be appropriately translated in the existence of standing waves of the corresponding discrete NLS models. The reader should be cautioned however that the stability properties in the latter context may differ [a relevant example will be discussed later in the text].

Our presentation will be structured as follows. In section II, we present the two discrete models and some of their basic properties. In section III, we discuss the details of the construction of the general exact static solutions of the models both in the localized (hyperbolic function) and in the extended (general elliptic function) form, and for both signs of the nonlinearity prefactor λ . $\lambda = 1$ corresponds to the so-called defocusing case, while $\lambda = -1$ corresponds to the focusing case in the standard terminology of NLS equations. Examples of the solutions are then given in section IV. In section V, we analyze the stability of the obtained solutions. In section VI, slow kink dynamics in the PNp-free models is compared numerically with that in the classical ϕ^4 model. In section VII we give a complete list of bounded and unbounded exact solutions to the continuum ϕ^4 field. In section VIII, we summarize our findings and present our conclusions.

II. TWO PNp-FREE DISCRETE ϕ^4 MODELS

At first, we consider the first integral of the static version of Eq. (3),

$$u(x) \equiv \phi_x^2 - \frac{\lambda}{2}(1 - \phi^2)^2 + C = 0, \quad (6)$$

where C is the integration constant. For our present purposes it is sufficient to take the following two-point discretization of Eq. (6)

$$u(\phi_{n-1}, \phi_n) \equiv \frac{1}{h^2}(\phi_n - \phi_{n-1})^2 - \frac{\lambda}{2}(1 - \phi_{n-1}\phi_n)^2 + C = 0, \quad (7)$$

although more general expressions can be constructed easily (see Eqs. (11) and (27) of [13]). Note that in an earlier study [13] we set $C = 0$ to obtain kink solutions; nevertheless, the key point of the present work is that we treat C as an arbitrary integration constant to obtain *all* possible solutions of the static model.

Let us denote

$$\Lambda = \lambda h^2, \quad \tilde{C} = Ch^2. \quad (8)$$

Then, discretizing the left-hand side of the identity $(1/2)d\psi/d\phi = D(x; t)$, we obtain the following discrete

version of Eq. (3)

$$\begin{aligned}\ddot{\phi}_n &= \frac{u(\phi_n, \phi_{n+1}) - u(\phi_{n-1}, \phi_n)}{\phi_{n+1} - \phi_{n-1}} \\ &= \frac{1}{h^2}(\phi_{n-1} - 2\phi_n + \phi_{n+1}) \\ &+ \lambda\phi_n - \frac{\lambda}{2}\phi_n^2(\phi_{n-1} + \phi_{n+1}).\end{aligned}\quad (9)$$

This non-Hamiltonian PNp-free ϕ^4 model conserves the momentum \mathcal{P} [11, 13] which has the form:

$$\mathcal{P} = \sum_n \dot{\phi}_n(\phi_{n+1} - \phi_{n-1}), \quad (10)$$

and it will be referred to as the momentum-conserving (MC) model.

To find the equilibrium solutions of Eq. (9), formally we need to solve the three-point difference equation, but it is clear that the solutions can equivalently be found from the reduced two-point problem $u(\phi_{n-1}, \phi_n) = 0$, [see Eq. (7)].

As was described in [13], a PNp-free model can be transformed to another PNp-free model by multiplying the corresponding static equation by a function $e(h, \phi_{n-1}, \phi_n, \phi_{n+1})$ possessing a continuum limit equal to 1. Such multiplication will not change either the continuum limit, or the static solutions of the model, provided that $e(h, \phi_{n-1}, \phi_n, \phi_{n+1}) = 0$ has no solutions.

Following the above concept, we multiply the right-hand side of Eq. (9) by $e(h, \phi_n) = 1/(1 - \Lambda\phi_n^2/2)$, to derive the following PNp-free model discovered in [15],

$$\ddot{\phi}_n = \frac{1}{h^2}(\phi_{n-1} - 2\phi_n + \phi_{n+1}) + \frac{\lambda(\phi_n - \phi_n^3)}{1 - \Lambda\phi_n^2/2}, \quad (11)$$

having the same static solutions [derivable from Eq. (7)] as the model of Eq. (9). The model of Eq. (11) will be called the energy-conserving (EC) model because it possesses the Hamiltonian [15]

$$\mathcal{H} = \frac{1}{2} \sum_n \left[\dot{\phi}_n^2 + \frac{(\phi_n - \phi_{n-1})^2}{h^2} + V(\phi_n) \right], \quad (12)$$

where the potential $V(\phi_n)$ is given by

$$V(\phi_n) = -\frac{1}{h^2} \left(\phi_n^2 + \frac{2 - \Lambda}{\Lambda} \ln \left| 1 - \frac{\Lambda\phi_n^2}{2} \right| \right). \quad (13)$$

In Fig. 1 we plot the potential $V(\phi_n)$ for $h = 1$ (i.e., $\Lambda = \lambda$) in both cases $\lambda = 1$ (solid line) and $\lambda = -1$ (dashed line). For $\lambda < 0$ the potential is smooth and it has one minimum at $\phi_n = 0$ and two maxima at $\phi_n = \pm 1$. For $\lambda > 0$ the potential has two minima at $\phi_n = \pm 1$ and a maximum at $\phi_n = 0$; note that in the limit $\phi_n \rightarrow \pm\sqrt{2/\Lambda}$, the potential $V(\phi_n) \rightarrow +\infty$.

It is not possible to plot an analog of Fig. 1 for the MC model since the relevant background forces are of many-body type (i.e., involve nearest neighbors) and are non-potential.

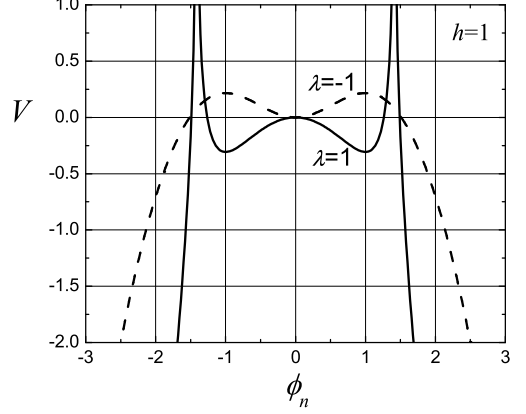


FIG. 1: The on-site potential of the EC model of Eq. (11), $V(\phi_n)$, defined by Eq. (13), for $h = 1$ and $\Lambda = \lambda = 1$ (solid line) and $\Lambda = \lambda = -1$ (dashed line). For $\lambda < 0$ the potential is smooth and it has one minimum at $\phi_n = 0$ and two maxima at $\phi_n = \pm 1$. For $\lambda > 0$ the potential has two minima at $\phi_n = \pm 1$ and a maximum at $\phi_n = 0$; as $\phi_n \rightarrow \pm\sqrt{2/\Lambda}$ the potential $V(\phi_n) \rightarrow +\infty$.

III. EXACT STATIC SOLUTIONS FOR DISCRETE MODELS

A. Solutions from nonlinear map

To find *all* static solutions to the PNp-free models of Eq. (9) and Eq. (11) we solve Eq. (7):

$$\begin{aligned}\phi_n &= \frac{(2 - \Lambda)\phi_{n-1} \pm \sqrt{\mathcal{D}}}{2 - \Lambda\phi_{n-1}^2}, \\ \mathcal{D} &= 2\Lambda(1 - \phi_{n-1}^2)^2 + 2\tilde{C}(\Lambda\phi_{n-1}^2 - 2),\end{aligned}\quad (14)$$

where ϕ_n and ϕ_{n-1} can be interchanged due to the symmetry of the equation. Starting from any admissible “initial” value ϕ_0 , by iterating Eq. (14) and its counterpart written as $\phi_{n-1} = f(\phi_n)$, one can construct recurrently the static solution to both the MC model of Eq. (9) and the EC model of Eq. (11), or to a linear combination thereof. Arbitrariness in the choice of ϕ_0 implies the absence of PNp in these models.

As can be seen from Eq. (14), there are certain restrictions on the choice of the values ϕ_0 . In particular, inadmissible initial values are those for which the denominator becomes zero, i.e., $\phi_0 \neq \pm\sqrt{2/\Lambda}$ for $\lambda > 0$, and also ones for which $\mathcal{D} < 0$. The condition $\mathcal{D} = 0$ leads to a biquadratic algebraic equation determining the borders of admissible region; the roots of this equation are:

$$(\phi_0^2)_{1,2} = 1 - \frac{\tilde{C}}{2} \pm \sqrt{\frac{\tilde{C}}{4} \left(\tilde{C} - 4 + \frac{8}{\Lambda} \right)}. \quad (15)$$

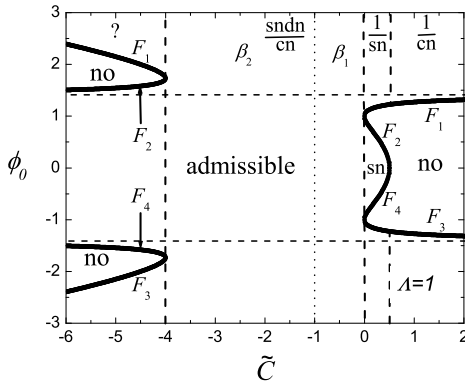


FIG. 2: Admissible region for the “initial” value ϕ_0 in the nonlinear map Eq. (14) for different values of \tilde{C} at $\Lambda = 1$. There are three inadmissible regions marked with “no” and two inadmissible lines $\phi_0 \neq \pm\sqrt{2}/\Lambda$ (horizontal dashed lines). On these lines the on-site potential $V(\phi_n)$ diverges (see Fig. 1). F_i ($i = 1, \dots, 4$) designate different branches of the borders of the admissible regions [see Eq. (15) and Eq. (16)]. Roots F_1 and F_2 merge at $\tilde{C} = 0$ and at $\tilde{C} = 4 - 8/\Lambda$. Roots F_2 and F_4 merge at $\tilde{C} = \Lambda/2$. Vertical dashed lines separate regions with different Jacobi elliptic function solutions. Vertical dotted line, situated (for the chosen parameters) at $\tilde{C}^* \approx -1.00$, divides the region of the sn/dn/cn solution into two portions corresponding to two roots of the first equation in Eq. (26).

Let us introduce the following notations for these roots:

$$F_1 = -F_3 = \sqrt{(\phi_0^2)_1}, \quad F_2 = -F_4 = \sqrt{(\phi_0^2)_2}. \quad (16)$$

The admissible regions for the values of ϕ_0 of the nonlinear map Eq. (14) are shown in Fig. 2 for different values of \tilde{C} at $\Lambda = 1$. The corresponding result for $\Lambda = -1$ is presented in Fig. 3. These graphs present a road map for constructing the various possible solutions of the above models.

The symmetry of Eq. (7) suggests that the topology of the admissible regions is such that once started from an admissible value of ϕ_0 , one cannot leave the admissible region iterating Eq. (14), so that the static solution will surely be constructed for the whole chain. This is so because Eq. (14) serves for calculating both back and forth points of the map, and if one is admissible, the other one is also admissible.

Equation (14) possesses two roots, which means that for an admissible initial condition one can construct two different solutions, e.g., a kink and an antikink. When iterating, to keep moving along the same solution, one must take ϕ_n different from ϕ_{n-2} [if the roots of Eq. (14) are different]. Indeed, setting in the three-point static

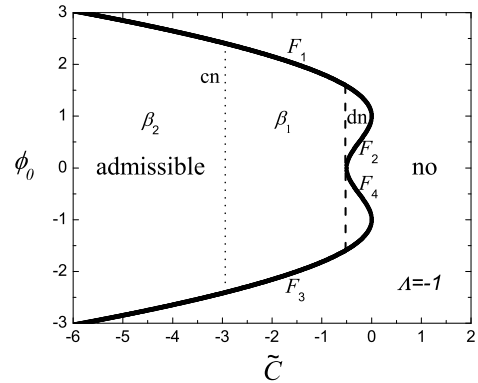


FIG. 3: Same as in Fig. 2 but for $\Lambda = -1$. Roots F_1 and F_2 merge at $\tilde{C} = 0$, and roots F_3 and F_4 merge at $\tilde{C} = \Lambda/2$. The dn solution, Eq. (23), is defined for $\Lambda/2 < \tilde{C} < 0$. The cn solution, Eq. (22), is defined for $\tilde{C} < \Lambda/2$, and this region is divided into two parts, β_1 and β_2 , each corresponding to a particular root of the first equation in Eq. (22). The border between these two regions is shown by the dotted line situated (for the chosen parameters) at $\tilde{C}^* \approx -2.96$.

problem, Eq. (9), $\phi_{n-1} = \phi_{n+1}$, we find

$$\phi_{n-1} = \frac{(2 - \Lambda)\phi_n}{2 - \Lambda\phi_n^2}. \quad (17)$$

Comparing this with Eq. (14), it is readily seen that the equilibrium in the three-point equation in the case of $\phi_{n-1} = \phi_{n+1}$ can be achieved only if $\mathcal{D} = 0$ and the two roots coincide. As mentioned above, the latter requirement is equivalent to the condition that ϕ_n is on the border of the admissible region.

As it can be deduced from Eq. (15), the topology of the admissible regions presented in Fig. 2 and Fig. 3 does not significantly change among different but positive and among different but negative values of Λ respectively; of course, one has to exclude also the particular case of $\Lambda = 2$ and the continuum limit (see Sec. VII). Here we will not discuss in detail the case of extremely high discreteness ($\Lambda > 2$), even though the analysis of this case does not present any additional difficulties.

To summarize, for any point of the admissible region, (\tilde{C}, ϕ_0) (shown in Figs. 2 and 3), the nonlinear map of Eq. (14) generates different static solutions to the MC model of Eq. (9) and to the EC model of Eq. (11).

B. Jacobi elliptic function solutions

Static solutions to the discrete PNp-free models of Eq. (9) and Eq. (11) have been reported [15] in the form of the Jacobi elliptic functions, sn, cn, and dn [20]. Below, we will derive such solutions.

The general form of the solutions is

$$\begin{aligned}\phi_n &= \pm A \operatorname{sn}^q(Z, m) \operatorname{cn}^r(Z, m) \operatorname{dn}^s(Z, m), \\ Z &= \beta h(n + x_0),\end{aligned}\quad (18)$$

where $0 \leq m \leq 1$ is the modulus of the Jacobi elliptic functions, A and β are the parameters of the solution, and x_0 is the arbitrary initial position. Finally the integers q, r, s specify a particular form of the solution.

In the limit of $m = 1$, Eq. (18) reduces to the hyperbolic function form

$$\phi_n = \pm A \operatorname{tanh}^q(Z) \cosh^{-r-s}(Z), \quad (19)$$

and, in the limit of $m = 0$, to the trigonometric function form

$$\phi_n = \pm A \operatorname{sin}^q(Z) \cos^r(Z). \quad (20)$$

Substituting the ansatz Eq. (18) into Eq. (7) we find that it can be satisfied for a limited number of combinations of integer powers q, r, s . For some of them, e.g., for $(q, r, s) = (1, -1, 0)$ and for $(q, r, s) = (1, -1, -1)$, we obtain imaginary amplitude A in the whole range of parameters.

Essentially different, real amplitude solutions described by Eq. (18), have the following form and are characterized by the following parameters:

The sn solution, $(q, r, s) = (1, 0, 0)$,

$$\begin{aligned}\operatorname{cn}(\beta h) \operatorname{dn}(\beta h) &= 1 - \frac{\Lambda}{2}, \quad A = \sqrt{\frac{2m}{\Lambda}} \operatorname{sn}(\beta h), \\ \tilde{C} &= \frac{\Lambda}{2} \left(1 - \frac{A^4}{m}\right), \quad 0 < \tilde{C} < \frac{\Lambda}{2}.\end{aligned}\quad (21)$$

The cn solution, $(q, r, s) = (0, 1, 0)$,

$$\begin{aligned}\frac{\operatorname{cn}(\beta h)}{\operatorname{dn}^2(\beta h)} &= 1 - \frac{\Lambda}{2}, \quad A = \sqrt{\frac{-2m}{\Lambda}} \frac{\operatorname{sn}(\beta h)}{\operatorname{dn}(\beta h)}, \\ \tilde{C} &= \Lambda \frac{(1 - A^2)^2}{2 - \Lambda A^2}, \quad -\infty < \tilde{C} < \frac{\Lambda}{2}.\end{aligned}\quad (22)$$

The dn solution, $(q, r, s) = (0, 0, 1)$,

$$\begin{aligned}\frac{\operatorname{dn}(\beta h)}{\operatorname{cn}^2(\beta h)} &= 1 - \frac{\Lambda}{2}, \quad A = \sqrt{\frac{-2}{\Lambda}} \frac{\operatorname{sn}(\beta h)}{\operatorname{cn}(\beta h)}, \\ \tilde{C} &= \Lambda \frac{(1 - A^2)^2}{2 - \Lambda A^2}, \quad \frac{\Lambda}{2} < \tilde{C} < 0.\end{aligned}\quad (23)$$

The 1/sn solution, $(q, r, s) = (-1, 0, 0)$,

$$\begin{aligned}\operatorname{cn}(\beta h) \operatorname{dn}(\beta h) &= 1 - \frac{\Lambda}{2}, \quad A = \sqrt{\frac{2}{\Lambda}} \operatorname{sn}(\beta h), \\ \tilde{C} &= \frac{\Lambda}{2} (1 - mA^4), \quad 0 < \tilde{C} < \frac{\Lambda}{2}.\end{aligned}\quad (24)$$

The 1/cn solution, $(q, r, s) = (0, -1, 0)$,

$$\begin{aligned}\frac{\operatorname{cn}(\beta h)}{\operatorname{dn}^2(\beta h)} &= 1 - \frac{\Lambda}{2}, \quad A = \sqrt{\frac{2(1-m)}{\Lambda}} \frac{\operatorname{sn}(\beta h)}{\operatorname{dn}(\beta h)}, \\ \tilde{C} &= \frac{\Lambda}{2} \left(1 + \frac{mA^4}{1-m}\right), \quad \frac{\Lambda}{2} < \tilde{C} < \infty.\end{aligned}\quad (25)$$

The sndn/cn solution, $(q, r, s) = (1, -1, 1)$,

$$\begin{aligned}\frac{m \operatorname{cn}^4(\beta h) + 1 - m}{\operatorname{cn}^2(\beta h)} &= 1 - \frac{\Lambda}{2}, \quad A = \sqrt{\frac{2}{\Lambda}} \frac{\operatorname{sn}(\beta h) \operatorname{dn}(\beta h)}{\operatorname{cn}(\beta h)}, \\ \tilde{C} &= \frac{\Lambda}{2} (1 - A^4), \quad 4 - \frac{8}{\Lambda} < \tilde{C} < 0.\end{aligned}\quad (26)$$

It is worth making the following remarks:

The solutions shown in Eq. (22) and Eq. (23) have real amplitudes for $\Lambda < 0$ while the others for $\Lambda > 0$.

The solutions should be interpreted in the following form. For a given Λ , one can find β by solving the first equation in Eqs. (21-26), and then A by solving the second one. Substituting these values in Eq. (18) results in the static solutions of the original discrete model.

The expressions for \tilde{C} in Eqs. (21-26) link the elliptic Jacobi function solutions and the solution in the form of the nonlinear map, Eq. (14). As for the other free parameter of the solutions Eq. (21-26), the arbitrary shift x_0 , its counterpart in the nonlinear map, Eq. (14), is effectively the initial value ϕ_0 .

The solutions of Eqs. (21-26) can be expressed in a number of other forms using the well-known identities for the Jacobi elliptic functions [20]. For example, shifting the argument by a quarter period, one can transform the sn solution to the form of cn/dn, or, applying the ascending Landen transformation, to the form of sncn/dn. Mathematically, these three expressions look as different members of Eq. (18), but physically they are indistinguishable.

IV. ANALYSIS OF STATIC SOLUTIONS

In what follows, we analyze the static solutions derivable from Eq. (14) discussing their relation to Eqs. (21)-(26). Since the topology of the admissible regions is different for positive and negative Λ , these two cases are studied separately.

A. $\Lambda > 0$ case.

In the sn solution, Eq. (21), when the elliptic modulus increases from its smallest value $m = 0$ to its largest value $m = 1$, the amplitude A increases from 0 to 1, since $A = F_2$ [see Eq. (15) and Eq. (16)]. As a result, the parameter \tilde{C} monotonically decreases from $\Lambda/2$ to 0. Thus, the sn solution is defined in the portion of the (\tilde{C}, ϕ_0) -plane, $0 \leq \tilde{C} \leq \Lambda/2$ and $|\phi_0| < F_2$ (see Fig. 2).

The 1/sn solution, Eq. (24), is defined for $0 \leq m \leq 1$, and it is complementary to the sn solution since it is also valid for $0 \leq \tilde{C} \leq \Lambda/2$, but for $|\phi_0| > F_1$ (see Fig. 2).

The 1/cn solution, Eq. (25), is defined for $0 \leq m \leq 1$ and it occupies the region $\Lambda/2 \leq \tilde{C} \leq \infty$, $|\phi_0| > F_1$ (see Fig. 2).

The sndn/cn solution, Eq. (26), is defined for unlimited ϕ_0 in the range $4 - 8/\Lambda \leq \tilde{C} \leq 0$ (see Fig. 2). This

solution is only valid for $m^* < m < 1$, where, for fixed λ , $m^*(h)$ is an increasing function of h and $m^*(0) = 1/2$. For $m < m^*$ the first expression in Eq. (26) does not have solutions for β . For $m^* < m < 1$, the equation has two roots, $\beta_1 < \beta_2$. For the limiting value, m^* , one can find the corresponding amplitude A^* from the second expression of Eq. (26), and then \tilde{C}^* , from the last expression. For the case of $\Lambda = 1$ presented in Fig. 2, we find $m^* \approx 0.933$ and $\tilde{C}^* \approx -1.00$.

It should be noticed that we have not found a solution of the form of Eq. (18) valid in the range of $\tilde{C} < 4 - 8/\Lambda$ (portion marked with the question mark in Fig. 2). It is likely that static solution in this range cannot be expressed in terms of the Jacobi elliptic functions because it does not survive in the continuum limit (see Sec. VII). However, the solution can easily be constructed from the nonlinear map in Eq. (14).

Let us now discuss further several particular examples of the above solutions. First of all, in the limit $m \rightarrow 1$ [see Eq. (19)], the sn solution, Eq. (21), reduces to the kink solution [15],

$$\phi_n = \pm \tanh[\beta h(n + x_0)], \quad (27)$$

while the 1/sn solution, Eq. (24), to the solution called hereafter the “inverted” kink,

$$\phi_n = \frac{\pm 1}{\tanh[\beta h(n + x_0)]}. \quad (28)$$

In Eqs. (27) and (28), x_0 is the (arbitrary) position of the solution and $\tanh(\beta h) = \sqrt{\Lambda/2}$.

This limiting case corresponds to $\tilde{C} = 0$, for which a heteroclinic connection is possible between the fixed points $\phi_n = -1$ and $\phi_n = 1$ (see Fig. 2), giving rise to the kink or the inverted kink. In this case, Eq. (14) assumes the following simple form

$$\phi_n = \frac{\phi_{n-1} \pm \sqrt{\Lambda/2}}{1 \pm \sqrt{\Lambda/2} \phi_{n-1}}, \quad (29)$$

where one can choose either the upper or the lower signs. The kink, Eq. (27), and the inverted kink, Eq. (28), can be derived from Eq. (29) taking initial values from $|\phi_0| < 1$ and $|\phi_0| > 1$, respectively.

In Fig. 4 we show (a) the kink and (b) the inverted kink solutions taking $\phi_0 = \sqrt{2} - 1$ and $\phi_0 = \sqrt{2} + 1$, respectively, for $\Lambda = 1$.

In Fig. 5, and for $\Lambda = 1$, we present two examples of solutions for positive and negative \tilde{C} close to 0. In particular, for $\tilde{C} = +2 \times 10^{-5}$, taking initial value $\phi_0 = 0$, we obtain from the map of Eq. (14) the solution presented in panel (a). In fact, it is the sn solution close to the hyperbolic function limit having the form of a periodic chain of kinks and anti-kinks. On the other hand, for $\tilde{C} = -6.75 \times 10^{-4}$ and $\phi_0 = 0$, we obtain from the map of Eq. (14) the solution shown in panel (b). This is the $\text{sn}dn/\text{cn}$ solution close to the hyperbolic function

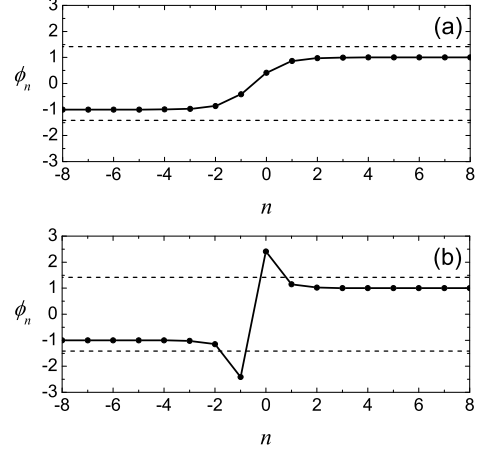


FIG. 4: Solutions at $\tilde{C} = 0$: (a) kink and (b) inverted kink at $\Lambda = 1$. Solutions can be found from the nonlinear map Eq. (29) with the initial conditions $\phi_0 = \sqrt{2} - 1$ and $\phi_0 = \sqrt{2} + 1$ for (a) and (b), respectively. The kink and the inverted kink are also given by Eqs. (27) and (28) respectively, for $x_0 = 0.5$. Horizontal dashed lines, $\phi_n = \pm \sqrt{2/\Lambda}$, show positions of singular points of the potential $V(\phi_n)$ (see Fig. 1).

limit and has a form of a chain of kinks and inverted anti-kinks.

In Fig. 6, and for $\Lambda = 1$, we present the 1/sn solution, Eq. (24), (a) close to the hyperbolic and (b) at the trigonometric limits. The solution shown in panel (a) is a chain of inverted kinks and inverted anti-kinks. These solutions are obtained from the nonlinear map Eq. (14) setting $\tilde{C} = 1.23 \times 10^{-9}$, $\phi_0 = 1 + \sqrt{2}$ for (a), and $\tilde{C} = 0.5$, $\phi_0 = 2.45$ for (b).

In summary, we have shown that the well-established (hyperbolic and elliptic function) solutions of the model correspond to a very narrow region of the two-parameter (ϕ_0, \tilde{C}) admissible space. A natural question is what is the typical profile outcome stemming from the use of other pairs of ϕ_0 and \tilde{C} in Eq. (14). We have found that one possibility consists of the inverted kinks and possible periodic generalizations thereof. Generically, upon testing the different regions of the admissible regime we have observed that arbitrary choices may lead to seemingly erratic solutions with very large amplitudes. A different sign choice in the right hand side of Eq. (14) may, however, lead to a periodically locked tail structure. A simple example of such a solution is given below.

B. $\Lambda < 0$ case.

For negative Λ , we have the cn solution, Eq. (22), and the dn solution, Eq. (23).

Let us first start from the latter: When m increases

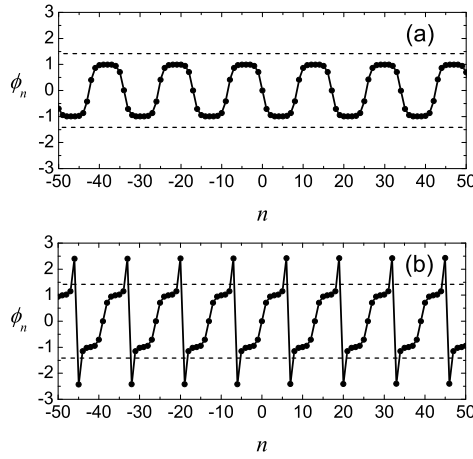


FIG. 5: Solutions for \tilde{C} close to 0, at $\Lambda = 1$, obtained from the map Eq. (14): (a) $\phi_0 = 0$, $\tilde{C} = 2 \times 10^{-5}$ and (b) $\phi_0 = 0$, $\tilde{C} = -6.75 \times 10^{-4}$. The solution in (a) is the sn solution, Eq. (21), and the solution in (b) is the sndn/cn solution, Eq. (26). Horizontal dashed lines, $\phi_n = \pm\sqrt{2/\Lambda}$, show positions of singular points of the potential $V(\phi_n)$ (see Fig. 1).

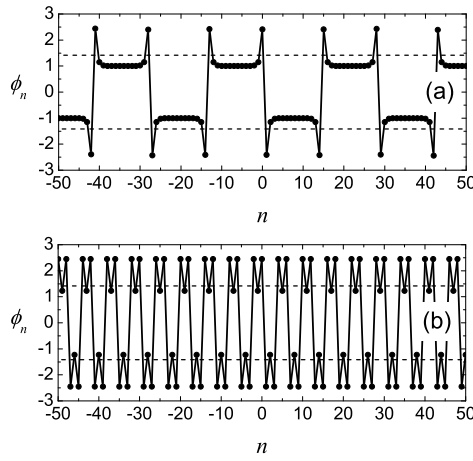


FIG. 6: The 1/sn solution, Eq. (24), (a) close to the hyperbolic and (b) at the trigonometric limits. We set $\Lambda = 1$. The solution in (a) consists of a chain of inverted kinks and inverted anti-kinks. To obtain these solutions from the nonlinear map Eq. (14) we set $\tilde{C} = 1.23 \times 10^{-9}$, $\phi_0 = 1 + \sqrt{2}$ for (a), and $\tilde{C} = 0.5$, $\phi_0 = 2.45$ for (b).

from 0 to 1 in Eq. (23), the parameter C decreases monotonically from 0 to $\Lambda/2$, i.e., this solution is defined in the “dn” portion of Fig. 3.

On the other hand, the cn solution of Eq. (22) is only valid for $m^* < m < 1$, where $m^*(h)$ is an increasing function of h and $m^*(0) = 1/2$. For $m < m^*$ the second

expression of Eq. (22) does not have solutions for β . For $m^* < m < 1$, the equation has two roots, $\beta_1 < \beta_2$. For the limiting value, m^* , one can find the corresponding amplitude A^* from the second expression of Eq. (22) and then \tilde{C}^* from the last expression. When m increases from m^* to 1 in Eq. (22), the parameter \tilde{C} of the nonlinear map Eq. (14) corresponding to the root β_1 (β_2) increases from \tilde{C}^* (decreases from \tilde{C}^*) to $\Lambda/2$ (to $-\infty$). Thus, the cn solution occupies the rest of the admissible region for the case of $\Lambda < 0$ (see Fig. 3). In the case of $\Lambda = -1$ presented in Fig. 3, we find $m^* \approx 0.873$ and $\tilde{C}^* \approx -2.96$.

Both cn and dn solutions, in the limit $m \rightarrow 1$ ($\tilde{C} \rightarrow \Lambda/2$), reduce to an homoclinic to 0 pulse solution (see also Figs. 1 and 3 where this possibility is illustrated). This solution has the form:

$$\phi_n = \pm A \operatorname{sech}[\beta h(n + x_0)], \quad (30)$$

where

$$\cosh(\beta h) = 1 - \frac{\Lambda}{2}, \quad \text{and} \quad A = \sqrt{2 - \frac{\Lambda}{2}}. \quad (31)$$

This is illustrated by Fig. 7 where, taking $\Lambda = -1$, we show the solution obtained from the map Eq. (14) at (a) $\tilde{C} = \Lambda/2 - 10^{-8}$ (dn solution) and (b) $\tilde{C} = \Lambda/2 + 10^{-8}$ (cn solution), for initial value of $\phi_0 = 10^{-4}$. The figure clearly illustrates the two limits (to the left and to the right of $\tilde{C} = \Lambda/2$) and their correspondence to pairs of pulse-pulse solutions and ones of pulse-anti-pulse solutions, as one enters the two different regimes “dn” and “cn” of Fig. 3.

C. Solutions with $\phi_{n-1} = \phi_{n+1}$

Solutions of this special form can be expressed as $\phi_n = A \cos(\pi n) + B$ with constant A and B . For the sake of simplicity, we set $B = 0$ and substitute the ansatz into Eq. (9) or Eq. (11) to find the zigzag solution

$$\phi_n = A \cos(\pi n), \quad A = \sqrt{\frac{4}{\Lambda} - 1}. \quad (32)$$

To obtain this solution from the map Eq. (14), one has to set $\tilde{C} = (\lambda/2)(1 + A^2)^2 - 4A^2/h^2$, which is the general condition for getting $\phi_n = -\phi_{n-1}$. Substituting here A from Eq. (32), we get $\tilde{C} = 4(\Lambda - 2)/(\Lambda h^2)$. For the case of $\Lambda = 1$ presented in Fig. 2, we have $\tilde{C} = -4$.

The zigzag solution is an exceptional one, as $\phi_n = \phi_{n-2}$ for any n . However, as shown above, this is only possible when Eq. (14) has multiple roots, which means that the two-point static problem, Eq. (7), is factorized. This solution does not have a counterpart in the continuum limit.

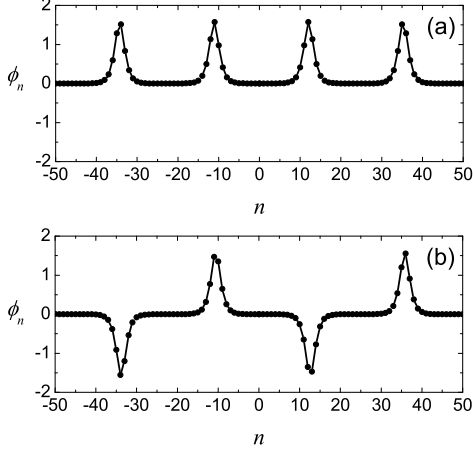


FIG. 7: Solutions for $\Lambda = -1$ at (a) $\tilde{C} = \Lambda/2 - 10^{-8}$ and (b) $\tilde{C} = \Lambda/2 + 10^{-8}$, for initial value of $\phi_0 = 10^{-4}$. Since \tilde{C} is close to $\Lambda/2 = -1/2$, corresponding to $m = 1$, the dn solution in (a) and the cn solution in (b) look like chains of separated pulses given by Eq. (30).

V. LINEAR STABILITY

The static solutions of the discrete models Eq. (9) and Eq. (11) are exactly the same, but the dynamical properties of the two models are different. As the corresponding stability analysis takes into account the dynamical form of each model, it will be carried out separately for each of the two.

Let us first consider the MC model of Eq. (9). Introducing the ansatz $\phi_n(t) = \phi_n^0 + \varepsilon_n(t)$ (where ϕ_n^0 is an equilibrium solution and $\varepsilon_n(t)$ is a small perturbation), we linearize Eq. (9) with respect to ε_n and obtain the following equation:

$$\ddot{\varepsilon}_n = \frac{1}{h^2}(\varepsilon_{n-1} - 2\varepsilon_n + \varepsilon_{n+1}) + \lambda\varepsilon_n - \frac{\lambda}{2}(\phi_n^0)^2(\varepsilon_{n-1} + \varepsilon_{n+1}) - \lambda\phi_n^0(\phi_{n-1}^0 + \phi_{n+1}^0)\varepsilon_n. \quad (33)$$

For the small-amplitude phonons, $\varepsilon_n = \exp(i\kappa n + i\omega t)$, with frequency ω and wave number κ , Eq. (33) is reduced to the following dispersion relation:

$$\omega^2 = \left[\frac{\lambda}{2}(\phi_n^0)^2 - \frac{1}{h^2} \right] \left(2 - 4 \sin^2 \frac{\kappa}{2} \right) + \frac{2}{h^2} - \lambda + \lambda\phi_n^0(\phi_{n-1}^0 + \phi_{n+1}^0). \quad (34)$$

From Eq. (34), the spectrum of the vacuum solutions for $\lambda > 0$, $\phi_n^0 = \pm 1$, is

$$\omega^2 = 2\lambda + \left(\frac{4}{h^2} - 2\lambda \right) \sin^2 \left(\frac{\kappa}{2} \right), \quad (35)$$

while the spectrum of the vacuum solution for $\lambda < 0$, $\phi_n^0 = 0$, is

$$\omega^2 = \frac{4}{h^2} \sin^2 \left(\frac{\kappa}{2} \right) - \lambda. \quad (36)$$

The stationary solution ϕ_n^0 is stable in the MC model if the eigenvalue problem Eq. (34) has only non-negative solutions ω^2 . Recalling that the MC model is a non-Hamiltonian one, this requirement leads to a non-self-adjoint eigenvalue problem involving a non-symmetric matrix.

Similarly, we obtain analogous expressions for the EC model of Eq. (11). The linearized equation reads

$$\ddot{\varepsilon}_n = \frac{1}{h^2}(\varepsilon_{n-1} - 2\varepsilon_n + \varepsilon_{n+1}) + 2\lambda \frac{2 + (\Lambda - 6)(\phi_n^0)^2 + \Lambda(\phi_n^0)^4}{[2 - \Lambda(\phi_n^0)^2]^2} \varepsilon_n, \quad (37)$$

and the corresponding dispersion relation for the linear phonon modes has the form:

$$\omega^2 = \frac{4}{h^2} \sin^2 \left(\frac{\kappa}{2} \right) - 2\lambda \frac{2 + (\Lambda - 6)(\phi_n^0)^2 + \Lambda(\phi_n^0)^4}{[2 - \Lambda(\phi_n^0)^2]^2}. \quad (38)$$

Hence, the spectrum of vacuum solutions $\phi_n = \pm 1$ (for $\lambda > 0$) is

$$\omega^2 = \frac{4\lambda}{2 - \Lambda} + \frac{4}{h^2} \sin^2 \left(\frac{\kappa}{2} \right), \quad (39)$$

while that of vacuum solution $\phi_n = 0$ (for $\lambda < 0$) is

$$\omega^2 = \frac{4}{h^2} \sin^2 \left(\frac{\kappa}{2} \right) - \lambda. \quad (40)$$

The stationary solution ϕ_n^0 is stable in the EC model of Eq. (11) if the self-adjoint eigenvalue problem of Eq. (38) has only non-negative solutions ω^2 .

We note that all stable and unstable static solutions of the MC and the EC models, except for the zigzag solution Eq. (32), possess a zero-frequency mode. This is a consequence of the effective translational invariance of the discrete PNp-free models; this is related also to the freedom of selecting the free parameter x_0 in the corresponding solution expressions.

Our aim here is not to study the whole bunch of solutions in the whole range of parameters, but rather to demonstrate the existence of stable solutions and also provide some examples where solutions, being stable in one model, may be unstable in another.

First, we consider the kink and inverted kink solutions given in Eq. (27) and Eq. (28) respectively: In a numerical experiment, these solutions were placed in the middle of chain of $N = 200$ particles with clamped boundary conditions. We have found that for the chosen set of parameters, the kink is stable in both MC and EC models,

while the inverted kink is stable in the EC and unstable in the MC model.

In Fig. 8 we show the spectra of the kink and the inverted kink for their different positions with respect to the lattice, x_0 . In the figure, the horizontal lines show the borders of the phonon band of the vacuum $\phi_n = \pm 1$ and the dots show the frequencies of the kink's internal modes lying outside of the band. In all cases, the spectra are shown as functions of x_0 , even though, admittedly, the kink in the MC model presented in (a) demonstrates very weak sensitivity of its spectrum to variations of x_0 .

Let us now consider the periodic solutions depicted in Fig. 5(b) (sندn/cn) and in Fig. 6(a) (1/sn). Close to the hyperbolic function limit, these solutions are stable in the EC model but unstable in the MC model, following the stability of the building blocks (inverted kinks) entering these structures. On the other hand, the 1/sn solution becomes unstable in both models at the trigonometric limit depicted in Fig. 6(b). Nonetheless, we find it remarkable that some of these “apparently non-smooth” solutions (or maybe more correctly, solutions apparently containing a non-smooth continuum limit) may be potentially stable in the discrete setting. It would be worthwhile to analyze the stability of such structures in more detail and as a function of their elliptic modulus m .

Next, we consider the zigzag solution, Eq. (32), which exists for $0 < \Lambda < 4$. It can be shown that this solution can be stable in the EC model: Indeed, substituting Eq. (32) into Eq. (38) we obtain the dispersion relation for the linear phonon modes, $\omega^2 = (4/h^2) \sin^2(\kappa/2) + 8/[h^2(2 - \Lambda)]$. The solution is stable when ω^2 are non-negative, i.e., when $\Lambda < 2$. Combining this with the existence condition we find that the zigzag solution exists and it is stable in the EC model for $0 < \Lambda < 2$. Note that this exceptional solution does not possess the zero frequency mode, as it can be seen from the above dispersion relation. The amplitude of the solution, $\sqrt{4/\Lambda - 1}$, is always greater than 1. The zigzag solution is always unstable in the MC model, a result that can similarly be demonstrated.

The sn, cn, and dn solutions were found to be generically unstable in both the MC and EC models.

The instability of the pulse solution of Eq. (30) can be analytically justified in the present setting. It can be easily inferred from the invariance of the solution with respect to x_0 that the eigenvector leading to the zero eigenvalue of Fig. 8 is proportional to $\partial\phi/\partial x_0$ (where ϕ is the pulse solution profile). This is an anti-symmetric eigenvector, given the pulse's symmetric (around its center) nature. But then, from Sturm-Liouville theory for discrete operators [19], there should be an eigenvalue such that $\omega^2 < 0$ with a symmetric (i.e., even) eigenvector, resulting in the instability of the relevant pulse solution. Our numerical simulations fully support this conclusion. The pulse solution was constructed by iterating Eq. (14) for $\Lambda < 0$, $\tilde{C} = \Lambda/2$, and $0 < \phi_0 < \sqrt{2 - \Lambda}/2$, or directly from Eq. (30). We found that for $\lambda = -1$ the pulse solution is unstable in both models and over a wide range of

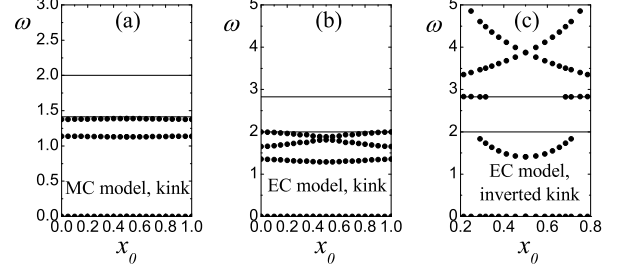


FIG. 8: Spectrum of (a) kink in MC model, (b) kink in EC model, and (c) inverted kink in EC model at $\tilde{C} = 0$, $\Lambda = 1$. The inverted kink in MC model is unstable for the chosen parameters. Horizontal lines show the borders of the phonon bands.

the discreteness parameter h , including the case of rather small $h \approx 0.1$. We have also confirmed that the instability mode is similar to the pulse profile (i.e., of even parity).

Both the cn and dn solutions (see, e.g., Fig. 7) are also found to be unstable for the different parameter values that we have used in both the MC and EC models. This is rather natural to expect given that their “building blocks”, namely the pulse-like solutions are each unstable (hence their concatenation will only add to the unstable eigendirections).

Finally, as far as the sn solutions are concerned, two basic instability modes were revealed. One resembles the instability of the pulse solution, when the whole structure, being waved around the top of the background potential, tends to slide down to one of the potential wells. The other instability modes can be understood if one regards the sn solution as a set of alternating kinks and anti-kinks [see Fig. 5(a)] interacting with each other by means of overlapping tails. Such a system is unstable because the kinks tend to annihilate with the anti-kinks.

It is interesting to note that these stability results suggest a disparity with the earlier numerical findings of [15] where the pulse-like solution was generically reported to be stable and analogous statements were made for the cn- and dn-type solutions.

At this point, it is worth discussing a connection with NLS-type models mentioned in the introduction. In the case of such models, the aforementioned unstable eigendirection (with an eigenvector similar in profile to the pulse itself) is “prohibited” by the additional conservation law of the L^2 norm, resulting in a separate neutral eigendirection with zero eigenfrequency. As a consequence, it is an interesting twist that the instability reported for such pulse-like solutions in scalar ϕ^4 models would be absent in their discrete NLS counterparts.

VI. SLOW KINK DYNAMICS

In [13], we have compared the spectra and the long-term dynamics of the kinks in the two PNp-free models, Eq. (9) and Eq. (11), with that of the classical discrete model, Eq. (4) (see Fig. 1 of that paper). In that study, kinks were boosted with the help of the translational eigenmodes found from the eigen-problem formulated in section V for the equations of motion linearized in the vicinity of the exact kink solution. The case of very small kink velocities was not studied there. Here we would like to focus on this case to demonstrate the qualitatively different behavior for slowly moving kinks in the PNp-free and classical models.

In Fig. 9 we present the lowest frequency normalized eigenmodes for the inter-site kinks in the three models, for the case of $h = 1$, $\lambda = 1$ ($\Lambda = 1$). Both PNp-free models, Eq. (9) and Eq. (11), have near identical translational eigenmodes with $\omega = 0$, shown by dots connected with solid lines. For the classical model, Eq. (4), the lowest-frequency mode has $\omega \approx 0.252$, and it is shown by open circles and dashed lines. Actually, this mode is not a translational mode (strictly speaking, since there is no translational invariance) but we use it to boost the kink.

We define the kink center of mass as

$$S = \frac{\sum_n n \sqrt{1 - \phi_n^2}}{\sum_n \sqrt{1 - \phi_n^2}}. \quad (41)$$

The evolution of the kink coordinates is shown in Fig. 10. Kinks were boosted with two different amplitudes of the normalized lowest-frequency eigenmodes, 0.02 and 0.08. Results for the PNp-free models practically coincide, as depicted by the dashed and solid lines for the MC and EC models, respectively. It is readily seen that kinks in the PNp-free lattices propagate with constant velocities.

The oscillatory trajectories in Fig. 10 correspond to the kink in the classical discrete ϕ^4 model. The faster kink, boosted with the amplitude of normalized lowest-frequency mode equal to 0.08, propagates along the lattice but its velocity gradually decreases. The kinetic energy of the translational motion is partly lost to the excitation of the kink internal mode with $\omega \approx 1.26$, laying below the phonon frequency band. Higher harmonics of this mode interact with the phonon spectrum producing radiation, which also slows the kink down. Even more dramatic difference is observed for the slower kinks, boosted at the amplitude of normalized lowest-frequency mode equal to 0.02. Here, the classical kink cannot overcome the PNp barrier and can not propagate, oscillating near the stable inter-site configuration. On the other hand, the kinks in the PNp-free models are not trapped by the lattice and propagate due to the absence of the PNp barrier. Alternatively, one can say that such waveforms can be accelerated by arbitrarily small external fields.

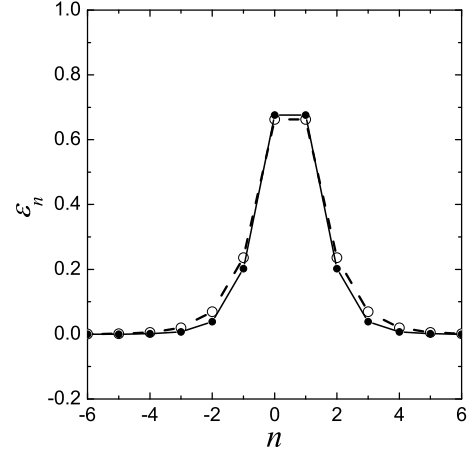


FIG. 9: Lowest frequency normalized eigenmodes for inter-site kinks. Both PNp-free models, Eq. (9) and Eq. (11), have very close (indistinguishable in the scale of this figure) translational eigenmodes with $\omega = 0$, shown by dots connected with solid lines. For the classical model, Eq. (4), the lowest-frequency mode has $\omega \approx 0.252$ (shown by open circles and dashed lines). Results for $h = 1$, $\lambda = 1$ ($\Lambda = 1$).

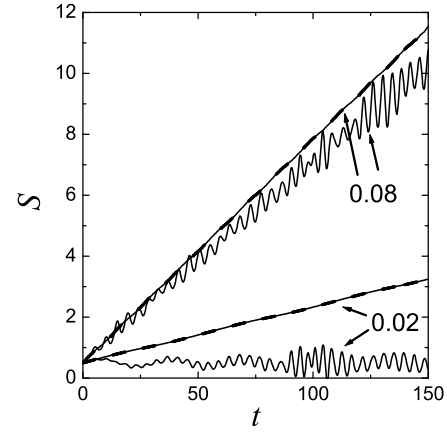


FIG. 10: Kink coordinate, S , as a function of time for kinks propagating in the PNp-free MC (dashed line) and EC (solid line) models, as well as in the classical discrete ϕ^4 model (oscillatory line). The kinks were boosted with two different amplitudes of the normalized lowest-frequency eigenmodes, 0.02 and 0.08. The faster classical kink is able to propagate, while the slower one is not, since it cannot overcome the PNp barrier. Kinks in PNp-free models are not trapped by the lattice and can propagate with any small velocity.

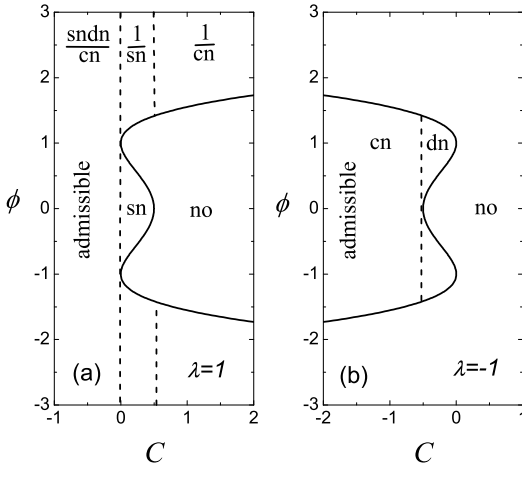


FIG. 11: Admissible regions for the ϕ^4 field for (a) $\lambda = +1$ and (b) $\lambda = -1$ obtained as the continuum limits ($h \rightarrow 0$) of that presented in Fig. 2 and Fig. 3, respectively. In each panel there is one inadmissible region marked with “no”.

VII. SOLUTIONS FOR CONTINUUM ϕ^4 FIELD

In the continuum limit, $h \rightarrow 0$, the borders of the admissible region, Eq. (15), become

$$(\phi_0^2)_{1,2} = 1 \pm \sqrt{\frac{2C}{\lambda}}. \quad (42)$$

In Fig. 11 we plot the admissible regions for (a) $\lambda = 1$ and (b) $\lambda = -1$. The topology of the admissible regions for the ϕ^4 field is simpler than the one pertaining to the discrete models. In the continuum limit there exists a sole inadmissible region for both cases $\lambda = \pm 1$, while three inadmissible regions exist for the discrete models in the case $\Lambda > 0$. One more simplification is that the domains of the sn/dn/cn and cn solutions do not split into two parts since the smaller root β_1 disappears in the continuum limit. Particularly we note that the region marked with the question mark in Fig. 2, $\tilde{C} < 4 - 8/\Lambda$, disappears in the continuum limit. That might be the reason why we failed to find a Jacobi elliptic function expression for the discrete static solutions in this case.

Static solutions Eqs. (21-26) obtained for the discrete models have their continuum counterparts as the traveling solutions to the ϕ^4 field, Eq. (3). The general form of the solutions is

$$\begin{aligned} \phi(x, t) &= \pm A \operatorname{sn}^q(z, m) \operatorname{cn}^r(z, m) \operatorname{dn}^s(z, m), \\ z &= \beta h(x + x_0) - \beta v t, \end{aligned} \quad (43)$$

where $0 \leq m \leq 1$ is the modulus of the Jacobi elliptic functions, A and β are the parameters of the solution, x_0 is the arbitrary initial position and $0 \leq v < 1$ is the

velocity of the solution. The integers q, r, s once again specify the particular form of the solution.

Continuum analogues of Eqs. (21)-(26) have the following form and are characterized by the following parameters:

The sn solution, $(q, r, s) = (1, 0, 0)$,

$$\begin{aligned} \beta &= \sqrt{\frac{\lambda}{(1+m)(1-v^2)}}, & A &= \sqrt{\frac{2m}{1+m}}, \\ C &= \frac{\lambda}{2} \left(1 - \frac{A^4}{m}\right), & 0 < C < \frac{\lambda}{2}. \end{aligned} \quad (44)$$

The cn solution, $(q, r, s) = (0, 1, 0)$,

$$\begin{aligned} \beta &= \sqrt{\frac{-\lambda}{(2m-1)(1-v^2)}}, & A &= \sqrt{\frac{2m}{2m-1}}, \\ C &= \frac{\lambda}{2} (1 - A^2)^2, & -\infty < C < \frac{\lambda}{2}. \end{aligned} \quad (45)$$

The dn solution, $(q, r, s) = (0, 0, 1)$,

$$\begin{aligned} \beta &= \sqrt{\frac{-\lambda}{(2-m)(1-v^2)}}, & A &= \sqrt{\frac{2}{2-m}}, \\ C &= \frac{\lambda}{2} (1 - A^2)^2, & \frac{\lambda}{2} < C < 0. \end{aligned} \quad (46)$$

The 1/sn solution, $(q, r, s) = (-1, 0, 0)$,

$$\begin{aligned} \beta &= \sqrt{\frac{\lambda}{(1+m)(1-v^2)}}, & A &= \sqrt{\frac{2}{1+m}}, \\ C &= \frac{\lambda}{2} (1 - mA^4), & 0 < C < \frac{\lambda}{2}. \end{aligned} \quad (47)$$

The 1/cn solution, $(q, r, s) = (0, -1, 0)$,

$$\begin{aligned} \beta &= \sqrt{\frac{\lambda}{(1-2m)(1-v^2)}}, & A &= \sqrt{\frac{2(1-m)}{1-2m}}, \\ C &= \frac{\lambda}{2} \left(1 + \frac{mA^4}{1-m}\right), & \frac{\lambda}{2} < C < \infty. \end{aligned} \quad (48)$$

The sn/dn/cn solution, $(q, r, s) = (1, -1, 1)$,

$$\begin{aligned} \beta &= \sqrt{\frac{\lambda}{2(2m-1)(1-v^2)}}, & A &= \frac{1}{\sqrt{2m-1}}, \\ C &= \frac{\lambda}{2} (1 - A^4), & -\infty < C < 0. \end{aligned} \quad (49)$$

The above six solutions can be rewritten in a great variety of forms using the properties of the Jacobi elliptic functions [20]. However, we believe that they may constitute the full list of physically different solutions to the continuum ϕ^4 equation since they fill the whole two-parameter space, (C, ϕ) , obtained as the continuum limit of corresponding space of the discrete model.

All solutions are conveniently parameterized by a single parameter $-\infty < C < \infty$ for $\lambda > 0$, and $-\infty < C \leq 0$ for $\lambda < 0$, as it is presented in Fig. 11.

The solutions in Eqs. (44)-(46) are bounded while the other ones are unbounded. The solutions in Eq. (45) and Eq. (46) are defined for $\lambda < 0$ while the others for $\lambda > 0$. The solutions in Eq. (45) and Eq. (49) are valid for $1/2 < m \leq 1$, the solution in Eq. (48) is valid for $0 \leq m < 1/2$, while the other solutions for $0 \leq m \leq 1$.

VIII. CONCLUSIONS

In the present paper we have shown that the reduction of the static problem of a discrete Klein-Gordon (and by extension of the standing wave problem of a discrete NLS) equation to a two-point problem is a powerful tool for obtaining all possible solutions of the corresponding model. We have applied this general idea to a momentum conserving [11] and an energy conserving [15] discretization of the ϕ^4 model analyzing the full two-parameter plane of solutions and giving a natural parameterization for it. In particular, we have examined the admissible regions of the field value at a given point and of the constant entering the two-point function pertinent to the model. We have specifically illustrated how to use different choices of these two parameters to obtain not only the well-known hyperbolic function solutions and the established elliptic function solutions, but also novel classes of solutions including the inverted (non-monotonic) kink solutions presented herein and multi-kink generalizations thereof. We performed such computations both for the attractive (focusing) and for the repulsive (defocusing) types of nonlinearity.

The presented methodology has the significant advan-

tage over earlier work that by introducing the integration constant in the discretization of the first integral of the static part of the PDE, it allows one to construct the *full* family of the static solutions of the corresponding model. Earlier work had implicitly set this additional free parameter to 0; this choice was sufficient for obtaining the important hyperbolic function solutions, but the present formalism systematically illustrates how to generalize the latter.

We have also derived the continuum analogues of the discrete solutions and found that they fill the whole space of parameters obtained in the limit of $h \rightarrow 0$ from the parameter space of the discrete models.

In addition, we have examined some of the key stability features of the solutions obtained in the various models, illustrating the different stability properties of the models considered herein (even if their static solutions are identical). We have obtained interesting stability properties, including, e.g., the counter-intuitive stability of the inverted kink and of some its periodic generalizations for the EC model.

The present study generates a variety of interesting questions. For instance, it would be relevant to examine whether the solutions presented herein (including the inverted ones) have counterparts in the “standard” discrete ϕ^4 model and to analyze their respective stability. It would also be relevant to examine how the stability (and existence –since some of them may not survive the continuum limit–) of such solutions depend on the lattice spacing h . Finally, these and related (e.g. stability) questions in the context of discrete NLS lattices would also be equally or even more (given the multitude of relevant applications of the latter model) interesting to answer. Such studies are currently in progress and will be reported elsewhere.

[1] O. M. Braun and Y. S. Kivshar, *The Frenkel-Kontorova Model: Concepts, Methods, and Applications* (Springer, Berlin, 2004).

[2] A. Scott, *Nonlinear Science: Emergence and Dynamics of Coherent Structures* (Oxford Univ. Press, Oxford, 2003).

[3] M. Toda, *Theory of Nonlinear Lattices* (Springer-Verlag, Berlin, 1981).

[4] M. J. Ablowitz and J. F. Ladik, *J. Math. Phys.* **16**, 598 (1975); M. J. Ablowitz and J. F. Ladik, *J. Math. Phys.* **17**, 1011 (1976).

[5] S. J. Orfanidis, *Phys. Rev. D* **18**, 3828 (1978).

[6] J. P. Hirth and J. Lothe, *Theory of Dislocations* (Krieger Publishing, Malabar, Florida, 1992).

[7] T. I. Belova and A. E. Kudryavtsev, *Phys. Usp.* **40**, 359 (1997).

[8] A. A. Aigner, A. R. Champneys and V. M. Rothos, *Physica D* **186**, 148 (2003).

[9] J. M. Speight, and R. S. Ward, *Nonlinearity* **7**, 475 (1994); J. M. Speight, *Nonlinearity* **10**, 1615 (1997); J. M. Speight, *Nonlinearity* **12**, 1373 (1999).

[10] E. B. Bogomol'nyi, *J. Nucl. Phys.* **24**, 449 (1976).

[11] P. G. Kevrekidis, *Physica D* **183**, 68 (2003).

[12] S. V. Dmitriev, P. G. Kevrekidis, and N. Yoshikawa, <http://arxiv.org/abs/nlin.PS/0506002>.

[13] S. V. Dmitriev, P. G. Kevrekidis, and N. Yoshikawa, *J. Phys. A* **38**, 7617 (2005).

[14] I. V. Barashenkov, O. F. Oxtoby, and D. E. Pelinovsky, *Phys. Rev. E* **72**, 35602R (2005).

[15] F. Cooper, A. Khare, B. Mihaila, and A. Saxena, *Phys. Rev. E* **72**, 36605 (2005).

[16] S. Aubry, *J. Chem. Phys.* **64**, 3392 (1976).

[17] J. M. Speight and Y. Zolotaryuk, [nlin.PS/0509047](http://arxiv.org/abs/nlin.PS/0509047).

[18] M. J. Ablowitz, B. Prinari and A. D. Trubatch, *Discrete and continuous nonlinear Schrödinger systems*, (Cambridge Univ. Press, Cambridge, 2004).

[19] H. Levy and F. Lessman, *Finite Difference Equations* (Dover, New York, 1992).

[20] *Handbook of mathematical functions*, edited by M. Abramowitz and I. A. Stegun (U. S. GPO, Washington, D.C., 1964).